Frontiers of Information Technology & Electronic Engineering
www.jzus.zju.edu.cn; engineering.cae.cn; www.springerlink.com
ISSN 2095-9184 (print); ISSN 2095-9230 (online)
E-mail: jzus@zju.edu.cn

Coverage performance of the multilayer UAV-terrestrial HetNet with CoMP transmission scheme*

Weihao WANG, Yifan JIANG, Zesong FEI, Jing GUO‡

School of Information and Electronics, Beijing Institute of Technology, Beijing 100081, China

E-mail: weihaowang@bit.edu.cn; jiangyifan@bit.edu.cn; feizesong@bit.edu.cn; jingguo@bit.edu.cn

Received June 30, 2021; Revision accepted Nov. 17, 2021; Crosschecked Dec. 9, 2021

Abstract: To support the ubiquitous connectivity requirement of sixth generation communication, unmanned aerial vehicles (UAVs) play a key role as a major part of the future communication networks. One major issue in UAV communications is the interference resulting from spectrum sharing and line-of-sight links. Recently, the application of the coordinated multipoint (CoMP) technology has been proposed to reduce the interference in the UAV-terrestrial heterogeneous network (HetNet). In this paper, we consider a three-dimensional (3D) multilayer UAV-terrestrial HetNet, where the aerial base stations (ABSs) are deployed at multiple different altitudes. Using stochastic geometry, we develop a tractable mathematical framework to characterize the aggregate interference and evaluate the coverage probability of this HetNet. Our numerical results show that the implementation of the CoMP scheme can effectively reduce the interference in the network, especially when the density of base stations is relatively large. Furthermore, the system parameters of the ABSs deployed at higher altitudes dominantly influence the coverage performance of the considered 3D HetNet.

Key words: Unmanned aerial vehicle; Poisson point process; Coordinated multipoint (CoMP); Statistics of interference; Coverage performance

https://doi.org/10.1631/FITEE.2100310 **CLC number:** TN92

1 Introduction

Although the worldwide development of fifth generation (5G) communication has facilitated many applications, there is a series of rising use cases that 5G cannot support well; e.g., the future Industry X.0 paradigm requires larger connection density and higher spectral efficiency than the corresponding metrics of 5G (Akyildiz et al., 2020). Therefore, to satisfy these growing demands, both academia and industry around the world have launched research projects on sixth generation (6G) communication (Dang et al., 2020; Giordani et al., 2020). As a solution, the upcoming 6G communication is expected to support 10 times the connectivity density and 5–10 times the spectral efficiency of 5G (Zhang ZQ et al., 2019).

To achieve the target performance of 6G, the integrated network (including the airborne, satellite, cellular, and other constituents) is one of the most important technologies in 6G, where unmanned aerial vehicles (UAVs) play a vital role (Kishk et al., 2020; Saad et al., 2020). As aerial user equipment (UE), UAVs can provide robust navigation service and also exhibit good reliability, security, and thorough performance by connecting to the cellular network (Zeng et al., 2019b). As mobile relays, UAVs can provide short-range line-of-sight (LoS) channels, which are more beneficial for the transmission of signals than the ground-to-ground (G2G) relay nodes (Li B et al., 2018). As aerial base stations

‡ Corresponding author

* Project supported by the Beijing Natural Science Foundation, China (No. L202015), the National Natural Science Foundation of China (No. 62001029), and the Young Talents Supporting Project of China Association for Science and Technology

ORCID: Weihao WANG, https://orcid.org/0000-0002-4686-6294; Jing GUO, https://orcid.org/0000-0001-6752-6064

(ABSs), UAVs are able to establish communication links quickly and provide coverage for hotspots and emergency situations (Li B et al., 2019; Kishk et al., 2020), which is in line with the development direction of the "intellicise" network (i.e., the network tends to be intelligence-endogenous and primitive-concise) (Zhang P et al., 2022). Specifically, ABSs carrying different types of communication equipment can be deployed in the whole three-dimensional (3D) space, forming the multilayer drone-cell heterogeneous network (HetNet) (Qiu et al., 2019). Owing to the flexibility and high mobility of UAVs, the multilayer drone-cell HetNet is able to serve diversified communication demands (e.g., different qualities of service requirements based on user densities) and support broad connectivity (Bor-Yaliniz and Yanikomeroglu, 2016). In addition, compared to the single-layer drone architecture, multilayer drones enable better spectral efficiency performance with stronger adaptability to various types of environments (Sekander et al., 2018).

Despite these advantages, there are some crucial challenges to be solved for the operation of the multilayer drone-cell HetNet. One major challenge to be addressed is the management of interference. In addition to the severe co-channel interference for scenarios in which spectrum sharing is supported (Sekander et al., 2018), LoS links can cause severe aerial-terrestrial interference during both uplink and downlink (Mei and Zhang, 2020). Some interference mitigation techniques for UAV-enabled networks have been investigated in the literature. Specifically, Jacovic et al. (2018) studied the intercarrier and intersymbol interference effects in urban environments and proposed a waveform design on the number of subcarriers to improve the bit error rate performance. To optimize the spectral efficiency, Singh et al. (2018) designed distributed algorithms based on UAV mobility and enhanced the inter-cell interference coordination and cell range expansion techniques. A cooperative non-orthogonal multiple access (NOMA) scheme was proposed by Mei and Zhang (2020) using the backhaul links among base stations (BSs) to mitigate the UAV's uplink interference with the data rate not greatly decreased.

Among current interference mitigation techniques, the coordinated multipoint (CoMP) technology has been considered an effective technique. The effectiveness of CoMP has been illustrated for terrestrial cellular networks (Irmer et al., 2011) and specified in the current long-term evolution (LTE)—Advanced Releases by the 3rd Generation Partnership Project (3GPP, 2011). Recently, some works have investigated the applications of CoMP in UAV networks. Li Y et al. (2020) proposed a 3D cellular architecture implementing the CoMP transmission technique on ABSs and aerial UEs based on the binominal point process in stochastic geometry. Liu et al. (2019) studied the optimization of UAV placement and movement for a multi-UAV-enabled multiuser system with CoMP implemented, and derived the bounds of user's average achievable rates. Using stochastic geometry, Zhang S and Liu (2018) derived the coverage probability and average achievable rate for a multi-UAV network, wherein two UAVs cooperated with each other to provide downlink transmission in postdisaster regions. These aforementioned research works focused only on the performance of UAV networks. Some other works also considered the applications of CoMP in the UAV-terrestrial HetNet. To be specific, Sun et al. (2019) proposed a user-centric cooperative scheme for a single UAV to serve ground users in malfunction areas, and derived the coverage probability and the spectral efficiency of the proposed scheme. Wu et al. (2018) proposed a cooperative UAV clustering mechanism for a 3D UAV-assisted terrestrial cellular network to offload ground users to UAVs, wherein energy harvesting and caching were implemented. In Wang XL et al. (2019a), an ABS-assisted cooperative system was considered, in which multiple ABSs relay downlink signals to users from a macro terrestrial BS (TBS) via non-coherent joint transmission, and the closed-form success probability of this system was analyzed. This work was further extended to an NOMA-enabled ABS-assisted cooperative network, and the outage probability was derived (Wang XL et al., 2019b).

However, most of the above works focused on the general design of the CoMP scheme on UAVs, while ignoring the impact of different UAV altitudes on the performance of CoMP in the UAV-terrestrial HetNet. Since the probability of links to be in LoS conditions is dependent mainly on the height of UAVs (Zeng et al., 2019a), it is necessary to take the deployment of ABSs in the vertical dimension into consideration when designing a CoMP scheme for ABSs. Moreover, most of the above works did not involve

the activation mechanism of the cooperative BSs, which can potentially improve the network performance (Tanbourgi et al., 2014a).

In this study, we focus on analyzing the coverage performance of a 3D multilayer UAV-terrestrial HetNet, in which ABSs are deployed at different altitudes. To reduce the interference in this network, a CoMP scheme based on non-coherent joint-transmission is implemented among TBSs and ABSs (Tanbourgi et al., 2014b), whereby multiple BSs satisfying certain conditions jointly transmit signals to users. In this way, the received signal strength on the user's side can be improved by combing the received signals non-coherently. The main contributions of this work are summarized below:

1. Based on stochastic geometry, we come up with a tractable mathematical framework to evaluate the n^{th} cumulant of the aggregate interference and the coverage performance of a multilayer UAV-terrestrial HetNet with a CoMP scheme. The results validate the accuracy of our proposed model for different numbers of layers.

2. The coverage probability is derived based on an approximation of the interference distribution in the network. The feasibility of the approximation is discussed and the accuracy is validated by our numerical results.

3. The impacts of ABS height and BS density on the coverage performance are investigated. We find that the incorporation of CoMP can reduce the interference effectively under the dense deployment of ABSs. Another important finding is that the system parameters of the higher-altitude ABSs constitute the main factor affecting the coverage performance.

2 System model

2.1 Spatial model

In this work, a multilayer 3D UAV-terrestrial HetNet is considered, which consists of TBSs, ABSs, and terrestrial UEs. The ABSs are assumed to be distributed on K planes with different heights H_k within a 3D space, where $k = 1, 2, ..., K$. For analytical tractability, the locations of ABSs in the k^{th} plane are modeled as an independent homogeneous Poisson point process (HPPP), denoted as $\Phi_k = \{y_{k,j}\}$, with density $\lambda_{\text{A},k}$, where $y_{k,j}$ represents the j^{th} ABS on the k^{th} plane. In addition, we assume that ABSs are hovering with a quasistationary state. The spatial locations of the TBSs are modeled as an independent HPPP with density λ_{T}, which can be represented by $\Phi_0 = \{y_{0,j}\}$, where $y_{0,j}$ denotes the j^{th} TBS. Note that the subscript k in Φ_k and $y_{j,k}$ is a non-negative integer in the range of zero to K, where $k = 0$ implies the TBS and $k \geq 1$ indicates the ABS. The spatial locations of the terrestrial users can be modeled as an independent HPPP. According to Slivnyak's theorem in stochastic geometry, the performance of a user located in a certain location can stand for the performance of a user at any location (Haenggi, 2012). Without loss of generality, the typical user is assumed at the origin. The universal frequency reuse mechanism is considered, and we further assume that each BS always has at least one UE to serve. Therefore, the typical user will receive interference from non-serving BSs. All the BSs and users are equipped with a signal antenna.

2.2 Channel model

In this study, there exist two types of links. One is the link from the TBS to the user, called the G2G link, and the other one is the link from the ABS to the user, called the air-to-ground (A2G) link. These two types of links are modeled as follows:

1. G2G link

The channel in the G2G link is modeled as the path loss plus block fading. For a specific G2G link, the power received by the user from the j^{th} TBS is

$$P_{\text{r}}(y_{0,j}) = P_{\text{t},0} K_{\text{r}} \eta_{\text{T}} g_{0,j,\text{T}} ||y_{0,j}||^{-\alpha_{\text{T}}}, \qquad (1)$$

where $P_{\text{t},0}$ represents the TBS transmit power, K_{r} represents the path loss at a reference distance of 1 m, η_{T} is the additional path loss of the G2G link (Alzenad and Yanikomeroglu, 2019), and $g_{0,j,\text{T}}$ is the independently and identically distributed (i.i.d.) fading power gain. Because there is a large amount of occlusions between TBSs and the typical user, Nakagami-m fading is assumed. Hence, $g_{0,j,\text{T}}$ follows Gamma distribution with a shape parameter m_{T} and a scale parameter $\frac{1}{m_{\text{T}}}$. $||y_{0,j}||$ is the distance between the j^{th} TBS and the typical user, where $||\cdot||$ is the distance measure. Furthermore, α_{T} represents the path loss exponent of the G2G link.

2. A2G link

We adopt the probabilistic transmission model to describe the A2G link (Al-Hourani et al., 2014; Zeng et al., 2019a). For example, the A2G link can

be either LoS or non-LoS (NLoS). The probability that an A2G link is an LoS transmission is specified by

$$p_{\mathrm{L}}(z_{k,j},H_k)=\frac{1}{1+A\mathrm{e}^{-B\left(\arctan\left(\frac{H_k}{z_{k,j}}\right)-A\right)}},\quad(2)$$

where H_k is the height of the k^{th} ABS plane, and $z_{k,j}$ is the Euclidean distance between the projection point of the j^{th} ABS of the k^{th} plane and the typical user on the horizontal plane. The constants A and B are environment parameters. Correspondingly, the probability that the A2G link is an NLoS transmission is $p_{\mathrm{N}}(z_{k,j},H_k)=1-p_{\mathrm{L}}(z_{k,j},H_k)$. Consequently, the received power of the typical user from ABS $y_{k,j}$ is a piece-wise function, expressed as

$$P_{\mathrm{r}}(y_{k,j})=\begin{cases}\dfrac{P_{\mathrm{t},k}K_{\mathrm{r}}\eta_{\mathrm{L}}g_{k,j,\mathrm{L}}}{||y_{k,j}||^{\alpha_{\mathrm{L}}}}, & p_{\mathrm{L}}\Big(\sqrt{||y_{k,j}||^2-H_k^2},H_k\Big),\\ \dfrac{P_{\mathrm{t},k}K_{\mathrm{r}}\eta_{\mathrm{N}}g_{k,j,\mathrm{N}}}{||y_{k,j}||^{\alpha_{\mathrm{N}}}}, & p_{\mathrm{N}}\Big(\sqrt{||y_{k,j}||^2-H_k^2},H_k\Big),\end{cases}\quad(3)$$

where $P_{\mathrm{t},k}$ represents the ABS transmit power on the k^{th} plane, and η_{L} (η_{N}) represents the additional path loss of the A2G link under LoS (NLoS) transmission condition. Furthermore, $g_{k,j,\mathrm{L}}$ ($g_{k,j,\mathrm{N}}$) is the i.i.d. fading power gain of the LoS (NLoS) transmission, which is assumed to follow Gamma distribution with a shape parameter m_{L} (m_{N}) and a scale parameter $\frac{1}{m_{\mathrm{L}}}$ ($\frac{1}{m_{\mathrm{N}}}$). α_{L} (α_{N}) is the path loss exponent of the A2G link under LoS (NLoS) transmission condition. By comparing Eqs. (1) and (3), we find that the received power shares the similar formulation except the subscripts T, L, and N, which describe the type of transmission link. For simplicity, in the following, we use symbol ι to represent the type of transmission link, where $\iota=\mathrm{T}$ denotes the G2G link, $\iota=\mathrm{L}$ denotes the LoS link, and $\iota=\mathrm{N}$ denotes the NLoS link.

2.3 CoMP transmission scheme

In this 3D UAV-terrestrial HetNet, TBSs and ABSs implement the non-coherent CoMP transmission scheme to provide downlink data transmission for terrestrial users. The network is assumed to work in a distributed manner. Compared with coherent CoMP transmission, synchronization among the cooperating BSs is less restrictive for non-coherent CoMP transmission, which is more practical for the coordination among BSs (Tanbourgi et al., 2014a, 2014b; Wang HM et al., 2018). The user-centric CoMP transmission scheme (Tanbourgi et al., 2014a, 2014b) is adopted in this work, including the following two steps: BS participation and cooperation activation.

1. At the BS participation step, some BSs are selected as candidate BSs for CoMP transmission. These candidate BSs need to meet the condition; i.e., the strength of the average received signal transmitted from the BS on the k^{th} plane with the link state ι, denoted as $y_{k,j,\iota}$, has to be larger than the cooperation threshold $\Theta_{k,\iota}$. Then, the candidate BSs forming a cooperative cluster can be denoted as

$$\mathcal{B}=\cup\mathcal{B}_{k,\iota},\quad(4)$$

$$\mathcal{B}_{k,\iota}\triangleq\left\{y_{k,j,\iota}\mid\|y_{k,j,\iota}\|\le D_{k,\iota}\triangleq\left(\frac{\Theta_{k,\iota}}{P_{\mathrm{t},k}K_{\mathrm{r}}\eta_\iota}\right)^{-\frac{1}{\alpha_\iota}}\right\},\quad(5)$$

where $\mathcal{B}_{k,\iota}$ is the collection of candidate BSs on the k^{th} plane with link state ι, and $||y_{k,j,\iota}||$ is the distance between BS $y_{k,j,\iota}$ and the typical user.

2. At the cooperation activation step, a part of the BSs from the cooperative cluster are selected to perform coordinated transmission to the typical user. The condition of selection is that the strength of the instantaneous received signal transmitted from the BS on the k^{th} plane with link state ι is larger than the activation threshold $\tilde{\Theta}_{k,\iota}$. The activated cooperative BSs form an activated cooperative cluster, denoted as

$$\mathcal{B}_{\mathrm{a}}=\cup\mathcal{B}_{\mathrm{a},k,\iota},\quad(6)$$

$$\mathcal{B}_{\mathrm{a},k,\iota}\triangleq\left\{y_{k,j,\iota}\in\mathcal{B}_{k,\iota}\mid\|y_{k,j,\iota}\|\le W_{k,\iota}(g_{k,j,\iota})\triangleq\left(\frac{\tilde{\Theta}_{k,\iota}}{P_{\mathrm{t},k}K_{\mathrm{r}}\eta_\iota g_{k,j,\iota}}\right)^{-\frac{1}{\alpha_\iota}}\right\},\quad(7)$$

where $\mathcal{B}_{\mathrm{a},k,\iota}$ is the set of activated cooperation BSs on the k^{th} plane with link state ι.

After the two steps corresponding to Eqs. (4) and (6), the associated BSs for the typical user (i.e., $\mathcal{B}_{\mathrm{a}}$) can be successfully determined.

3 Coverage probability analysis

3.1 Coverage probability metric

This work adopts the coverage probability as the metric to evaluate the network performance. The

definition of this metric is the probability that the signal-to-interference ratio (SIR) at the typical user is larger than a certain threshold τ, i.e.,

$$P_{\rm cov} \triangleq \Pr(\mathrm{SIR} > \tau) = \Pr\Big(\frac{S}{I_{\rm agg}}\Big), \tag{8}$$

where S is the instantaneous received signal power from the CoMP BSs and $I_{\rm agg}$ denotes the instantaneous aggregate interference from non-CoMP BSs. Before quantifying the received desired signal power and the aggregate interference, we first re-categorize the distribution of BSs for analytical convenience.

According to the probabilistic transmission model, the probability that the link between ABS and the typical user is an LoS link is related to the distance between the ABS and the typical user. Therefore, based on the thinning theorem in stochastic geometry (Haenggi, 2012), the spatial distribution of ABSs at each height can be regarded as two independent inhomogeneous Poisson point processes (in-HPPPs). Thus, the spatial location of the BSs in the HetNet can be divided into the following $2K+1$ Poisson point processes (PPPs), $\Psi_{k,\iota}$:

1. $\Psi_{0,\mathrm{T}} = \Phi_0$

This point process is composed of all TBSs with constant density λ_{T}, which is the same as that of the original point process for TBSs.

2. $\Psi_{k,\mathrm{L}} = \{y_{k,j,\mathrm{L}}\},\ k = 1, 2, ..., K$

This point process is composed of ABSs in the $k^{\rm th}$ layer whose links with the typical user are LoS links, known as LoS-ABSs. According to the thinning theorem, the density of this point process is

$$\lambda_{k,\mathrm{L}}(y_{k,j,\mathrm{L}}) = \lambda_{\mathrm{A},k} p_{\mathrm{L}}\Big(\sqrt{\|y_{k,j,\mathrm{L}}\|^2 - H_k^2}, H_k\Big). \tag{9}$$

3. $\Psi_{k,\mathrm{N}} = \{y_{k,j,\mathrm{N}}\},\ k = 1, 2, ..., K$

This point process is composed of ABSs in the $k^{\rm th}$ layer whose links with the typical user are NLoS links, known as NLoS-ABSs. Then the density of this point process is

$$\lambda_{k,\mathrm{N}}(y_{k,j,\mathrm{N}}) = \lambda_{\mathrm{A},k} p_{\mathrm{N}}\Big(\sqrt{\|y_{k,j,\mathrm{N}}\|^2 - H_k^2}, H_k\Big). \tag{10}$$

For the considered non-coherent CoMP transmission scheme, the instantaneous received desired signal power is the summation of the signal power from each CoMP BS (the detailed derivation can be found in Tanbourgi et al. (2014b)). Then the instantaneous received desired signal power is

$$\begin{aligned} S = &\sum_{y_{0,j,\mathrm{N}} \in \mathcal{B}_{\mathrm{a},0,\mathrm{T}}} P_{\mathrm{t},0} K_{\mathrm{r}} \eta_{\mathrm{T}} g_{0,j,\mathrm{T}} \|y_{0,j,\mathrm{T}}\|^{-\alpha_{\mathrm{T}}} \\ &+ \sum_{k=1}^{K} \sum_{\iota \in \{\mathrm{L},\mathrm{N}\}} \sum_{y_{k,j,\iota} \in \mathcal{B}_{\mathrm{a},k,\iota}} P_{\mathrm{t},k} K_{\mathrm{r}} \eta_{\iota} g_{k,j,\iota} \|y_{k,j,\iota}\|^{-\alpha_{\iota}}. \end{aligned} \tag{11}$$

Correspondingly, under the re-organized PPPs mentioned above, the instantaneous aggregate interference is given by

$$\begin{aligned} I_{\rm agg} = &\sum_{y_{0,j,\mathrm{T}} \in \overline{\mathcal{B}}_{\mathrm{a},0,\mathrm{T}} \cup \overline{\mathcal{B}}_{0,\mathrm{T}}} P_{\mathrm{t},0} K_{\mathrm{r}} \eta_{\mathrm{T}} g_{0,j,\mathrm{T}} \|y_{0,j,\mathrm{T}}\|^{-\alpha_{\mathrm{T}}} \\ &+ \sum_{k=1}^{K} \sum_{\iota \in \{\mathrm{L},\mathrm{N}\}} \sum_{y_{k,j,\iota} \in \overline{\mathcal{B}}_{\mathrm{a},k,\iota} \cup \overline{\mathcal{B}}_{k,\iota}} P_{\mathrm{t},k} K_{\mathrm{r}} \eta_{\iota} g_{k,j,\iota} \|y_{k,j,\iota}\|^{-\alpha_{\iota}}, \end{aligned} \tag{12}$$

where $\overline{\mathcal{B}}_{k,\iota} = \frac{\Psi_{k,\iota}}{\mathcal{B}_{k,\iota}}$ and $\overline{\mathcal{B}}_{\mathrm{a},k,\iota} = \frac{\mathcal{B}_{k,\iota}}{\mathcal{B}_{\mathrm{a},k,\iota}}$.

It can be seen from the above formulas that the received desired signal and interference come from the BSs with different link states. For coverage performance analysis without CoMP, the desired signal comes only from an individual BS and we can use the distribution of the fading power gain on the desired link to conduct the analysis. However, this approach is not applicable for the CoMP scenario, where the desired signal comes from multiple BSs. Therefore, similar to previous works (Tanbourgi et al., 2014b; Wu et al., 2018), we first approximate the distribution of the aggregate interference by a well-known distribution (e.g., having a closed-form formula) and then compute the coverage based on this distribution approximation.

3.2 Interference characterization

Interference is a fusion of many variables. Hence, the exact distribution of the interference is very difficult to obtain. Instead, we decide to find a distribution that fits the interference distribution the best. To implement the distribution fitting, we first characterize the statistics of the aggregate interference and the $n^{\rm th}$ cumulant of aggregate interference as presented in Proposition 1.

Proposition 1 Under the system model considered in Section 2, the $n^{\rm th}$ cumulant of the aggregate interference $I_{\rm agg}$ is expressed in Eq. (13) at the top of next page, where the function $\mathcal{F}_{k,\iota}(x) \triangleq \Big(1 - \frac{x}{m_\iota}\Big)^{-m_\iota}$ and $E_{g_{k,\iota}}[\cdot]$ denotes the expectation with respect to the fading power gain $g_{k,\iota}$.

$$\begin{aligned}\mathrm{Cum}_{I_{\mathrm{agg}}}(n)=\frac{\mathrm{d}^n}{\mathrm{d}s^n}\Bigg(&-E_{g_{0,\mathrm{T}}}\left[\int_{\min\{D_{0,\mathrm{T}},W_{0,\mathrm{T}}(g_{0,\mathrm{T}})\}}^{D_{0,\mathrm{T}}}\left(1-\exp\left(sP_{\mathrm{t},0}K_{\mathrm{r}}\eta_{\mathrm{T}}g_{0,\mathrm{T}}z^{-\alpha_{\mathrm{T}}}\right)\right)2\pi\lambda_{\mathrm{T}}z\mathrm{d}z\right]\\&-\int_{D_{0,\mathrm{T}}}^{\infty}\left(1-\mathcal{F}_{0,\mathrm{T}}\left(sP_{\mathrm{t},0}K_{\mathrm{r}}\eta_{\mathrm{T}}z^{-\alpha_{\mathrm{T}}}\right)\right)2\pi\lambda_{\mathrm{T}}z\mathrm{d}z-\sum_{k=1}^{K}\sum_{\iota\in\{\mathrm{L},\mathrm{N}\}}\Bigg(E_{g_{k,\iota}}\Bigg[\int_{\min\left\{\sqrt{D_{k,\iota}^2-H_k^2},\sqrt{W_{k,\iota}^2(g_{k,\iota})-H_k^2}\right\}}^{\sqrt{D_{k,\iota}^2-H_k^2}}\Bigg(1\\&-\exp\left(\frac{sP_{\mathrm{t},k}K_{\mathrm{r}}\eta_{\iota}g_{k,\iota}}{\left(\sqrt{z^2+H_k^2}\right)^{\alpha_{\iota}}}\right)\Bigg)2\pi\lambda_{\mathrm{A},k}p_{\iota}(z,H_k)z\mathrm{d}z\Bigg]\\&+\int_{\sqrt{D_{k,\iota}^2-H_k^2}}^{\infty}\left(1-\mathcal{F}_{k,\iota}\left(sP_{\mathrm{t},k}K_{\mathrm{r}}\eta_{\iota}(z^2+H_k^2)^{-\frac{\alpha_{\mathrm{L}}}{2}}\right)\right)2\pi\lambda_{\mathrm{A},k}p_{\iota}(z,H_k)z\mathrm{d}z\Bigg)\Bigg)\Bigg|_{s=0}.\end{aligned}\tag{13}$$

Proof According to the relationship between the cumulant and the moment generating function (MGF), we can have the n^{th} cumulant of I_{agg} as

$$\mathrm{Cum}_{I_{\mathrm{agg}}}(n)=\frac{\mathrm{d}^n}{\mathrm{d}s^n}\ln\left(\mathcal{M}_{I_{\mathrm{agg}}}(s)\right)\big|_{s=0}.\tag{14}$$

Since $I_{\mathrm{agg}}=I_{0,\mathrm{T}}+\sum_{k=1}^{K}\sum_{\iota\in\{\mathrm{L},\mathrm{N}\}}I_{k,\iota}$, where $I_{k,\iota}$ denotes the interference from $\Psi_{k,\iota}$, we can decompose the MGF of the aggregate interference as

$$\mathcal{M}_{I_{\mathrm{agg}}}(s)=\mathcal{M}_{I_{0,\mathrm{T}}}(s)\prod_{k=1}^{K}\prod_{\iota\in\{\mathrm{L},\mathrm{N}\}}\mathcal{M}_{I_{k,\iota}}(s).\tag{15}$$

Based on the definition of MGF, following the Campbell theorem, we have the MGF of the interference from TBSs as

$$\begin{aligned}&\mathcal{M}_{I_{0,\mathrm{T}}}(s)\\&=E\left[\exp\left(s\sum_{y_{0,j,\mathrm{T}}\in\overline{\mathcal{B}}_{\mathrm{a},0,\mathrm{T}}\cup\overline{\mathcal{B}}_{0,\mathrm{T}}}\frac{P_{\mathrm{t},0}K_{\mathrm{r}}\eta_{\mathrm{T}}g_{0,j,\mathrm{T}}}{\|y_{0,j,\mathrm{T}}\|^{\alpha_{\mathrm{T}}}}\right)\right]\\&=E\left[\prod_{y_{0,j,\mathrm{T}}\in\overline{\mathcal{B}}_{\mathrm{a},0,\mathrm{T}}\cup\overline{\mathcal{B}}_{0,\mathrm{T}}}\exp\left(s\frac{P_{\mathrm{t},0}K_{\mathrm{r}}\eta_{\mathrm{T}}g_{0,j,\mathrm{T}}}{\|y_{0,j,\mathrm{T}}\|^{\alpha_{\mathrm{T}}}}\right)\right]\\&=\exp\Bigg(-E_{g_{0,\mathrm{T}}}\Bigg[\int_{0}^{D_{0,\mathrm{T}}}\left(1-\exp\left(\frac{sP_{\mathrm{t},0}K_{\mathrm{r}}\eta_{\mathrm{T}}g_{0,\mathrm{T}}}{z^{\alpha_{\mathrm{T}}}}\right)\right)\\&\quad\times1\left(z>W_{0,\mathrm{T}}(g_{0,\mathrm{T}})\right)2\pi\lambda_{\mathrm{T}}z\mathrm{d}z\\&\quad-\int_{D_{0,\mathrm{T}}}^{\infty}\left(1-\exp\left(sP_{\mathrm{t},0}K_{\mathrm{r}}\eta_{\mathrm{T}}g_{0,\mathrm{T}}z^{-\alpha_{\mathrm{T}}}\right)\right)2\pi\lambda_{\mathrm{T}}z\mathrm{d}z\Bigg]\Bigg),\end{aligned}\tag{16}$$

where $1(\cdot)$ denotes the indication function.

Similarly, the MGF of the interference from the ABSs on the k^{th} plane with link state ι is given by

$$\begin{aligned}&\mathcal{M}_{I_{k,\iota}}(s)\\&=E\left[\exp\left(s\sum_{y_{k,j,\iota}\in\overline{\mathcal{B}}_{\mathrm{a},k,\iota}\cup\overline{\mathcal{B}}_{k,\iota}}P_{\mathrm{t},k}K_{\mathrm{r}}\eta_{\iota}g_{k,j,\iota}\|y_{k,j,\iota}\|^{-\alpha_{\iota}}\right)\right]\\&=E\left[\prod_{y_{k,j,\iota}\in\overline{\mathcal{B}}_{\mathrm{a},k,\iota}\cup\overline{\mathcal{B}}_{k,\iota}}\exp\left(sP_{\mathrm{t},k}K_{\mathrm{r}}\eta_{\iota}g_{k,j,\iota}\|y_{k,j,\iota}\|^{-\alpha_{\iota}}\right)\right]\\&=\exp\Bigg(-E_{g_{k,\iota}}\Bigg[\int_{0}^{\sqrt{D_{k,\iota}^2-H_k^2}}\Bigg(1\\&\quad-\exp\left(sP_{\mathrm{t},k}K_{\mathrm{r}}\eta_{\iota}g_{k,\iota}\left(\sqrt{z^2+H_k^2}\right)^{-\alpha_{\iota}}\right)\Bigg)\\&\quad\times1\left(\sqrt{z^2+H_k^2}>W_{k,\iota}(g_{k,\iota})\right)2\pi\lambda_{\mathrm{A},k}p_{\iota}(z,H_k)z\mathrm{d}z\\&\quad-\int_{\sqrt{D_{k,\iota}^2-H_k^2}}^{\infty}\Bigg(1\\&\quad-\exp\left(sP_{\mathrm{t},k}K_{\mathrm{r}}\eta_{\iota}g_{k,\iota}\left(\sqrt{z^2+H_k^2}\right)^{-\alpha_{\iota}}\right)\Bigg)\\&\quad\times2\pi\lambda_{\mathrm{A},k}p_{\iota}(z,H_k)z\mathrm{d}z\Bigg]\Bigg).\end{aligned}\tag{17}$$

Note that the subscript j in $g_{k,j,\iota}$ is dropped since $g_{k,j,\iota}$ is independently and identically distributed. This applies to $y_{k,j,\iota}$ as well.

By combining Eqs. (16) and (17) with Eq. (15) and substituting Eq. (15) into Eq. (14), we can obtain the n^{th} cumulant of I_{agg} in Eq. (13).

Next, we need to determine the suitable distribution model that fits the probability distribution of I_{agg}. According to the literature (Haenggi and Ganti, 2009; Tanbourgi et al., 2014b), Gamma

distribution is a good approximation for the interference composed of BSs subject to the PPP. Besides that, Gamma distribution is convenient for deriving mathematical expressions. To see the suitability of Gamma distribution, Fig. 1 shows the probability density function (PDF) approximations for the aggregate interference under different well-known distributions, where the simulation results are generated for comparison purpose. The key parameters of these distributions can be determined from the n^{th} cumulant of the aggregate interference (Guo et al., 2014). It can be seen that, compared to other distributions, the Gamma distribution fits the distribution of the interference the best. In the following coverage probability analysis, we approximate the aggregate interference by the following Gamma distribution with the PDF given by

$$f_{I_{\text{agg}}}(i_{\text{agg}}) = \frac{i_{\text{agg}}^{\alpha-1}\exp\left(-i_{\text{agg}}/\beta\right)}{\Gamma[\alpha]\beta^{\alpha}}, \tag{18}$$

where $\Gamma[\cdot]$ is the Gamma function, $\alpha = \frac{(E[I_{\text{agg}}])^2}{\text{Var}[I_{\text{agg}}]}$, and $\beta = \frac{\text{Var}[I_{\text{agg}}]}{E[I_{\text{agg}}]}$. The mean and variance of the aggregate interference are given in the following corollary:

Corollary 1 The mean $E[I_{\text{agg}}]$ and variance $\text{Var}[I_{\text{agg}}]$ of the aggregate interference I_{agg} are given by

$$\begin{aligned} E[I_{\text{agg}}] =& \frac{2\pi\lambda_{\text{T}}P_{\text{t},0}K_{\text{r}}\eta_{\text{T}}}{\alpha_{\text{T}}-2} \\ &\times E_{g_{0,\text{T}}}\left[\frac{g_{0,\text{T}}}{\min\left\{D_{0,\text{T}},W_{0,\text{T}}(g_{0,\text{T}})\right\}^{\alpha_{\text{T}}-2}}\right] \\ &+\sum_{k=1}^{K}\sum_{\iota\in\{\text{L},\text{N}\}}E_{g_{k,\iota}}\left[\mu_{k,\iota}(Z_{k,\iota}(g_{k,\iota}))\right], \end{aligned} \tag{19}$$

$$\begin{aligned} \text{Var}[I_{\text{agg}}] =& \frac{\pi\lambda_{\text{T}}P_{\text{t},0}^2K_{\text{r}}^2\eta_{\text{T}}^2}{\alpha_{\text{T}}-1} \\ &\times E_{g_{0,\text{T}}}\left[\frac{g_{0,\text{T}}^2}{\min\left\{D_{0,\text{T}},W_{0,\text{T}}(g_{0,\text{T}})\right\}^{2\alpha_{\text{T}}-2}}\right] \\ &+\sum_{k=1}^{K}\sum_{\iota\in\{\text{L},\text{N}\}}E_{g_{k,\iota}}\left[\nu_{k,\iota}(Z_{k,\iota}(g_{k,\iota}))\right], \end{aligned} \tag{20}$$

where the functions $\mu_{k,\iota}(\cdot)$, $\nu_{k,\iota}(\cdot)$, and $Z_{k,\iota}(\cdot)$ are

$$\begin{aligned} \mu_{k,\iota}(Z) \triangleq& \int_{Z}^{\infty}P_{\text{t},k}K_{\text{r}}\eta_{\iota}g_{k,\iota}\left(\sqrt{z^2+H_k^2}\right)^{-\alpha_{\iota}} \\ &\times 2\pi\lambda_{\text{A},k}p_{\iota}(z,H_k)z\text{d}z, \end{aligned} \tag{21}$$

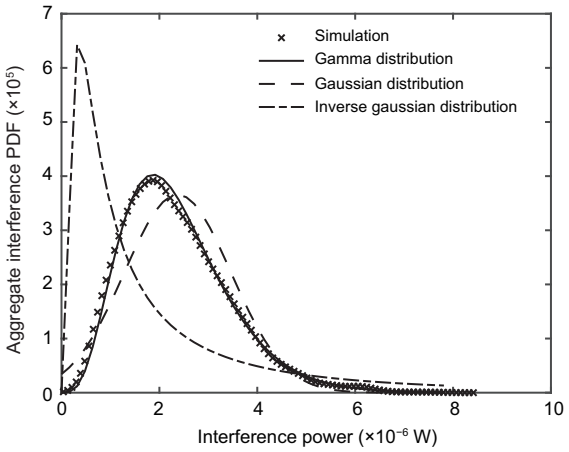

Fig. 1 Comparison of the probability density function (PDF) of several distributions and the result of simulation of interference

$$\begin{aligned} \nu_{k,\iota}(Z) \triangleq& \int_{Z}^{\infty}P_{\text{t},k}^2K_{\text{r}}^2\eta_{\iota}^2g_{k,\iota}^2\left(\sqrt{z^2+H_k^2}\right)^{-2\alpha_{\iota}} \\ &\times 2\pi\lambda_{\text{A},k}p_{\iota}(z,H_k)z\text{d}z, \end{aligned} \tag{22}$$

$$Z_{k,\iota}(g_{k,\iota}) \triangleq \begin{cases} \sqrt{W_{k,\iota}^2(g_{k,\iota})-H_k^2}, & H_k < W_{k,\iota}(g_{k,\iota}) < D_{k,\iota}, \\ \sqrt{D_{k,\iota}^2-H_k^2}, & H_k < D_{k,\iota} < W_{k,\iota}(g_{k,\iota}), \\ 0, & \text{otherwise}. \end{cases} \tag{23}$$

Proof The first cumulant and the second cumulant correspond to the mean and the variance, respectively. Therefore, according to Eq. (13), we can easily obtain the mean and the variance.

3.3 Formulation of coverage probability

Given that the probability distribution of the interference follows the Gamma distribution, according to Tanbourgi et al. (2014b), the approximated expression of the coverage probability is given in the following lemma:

Lemma 1 By letting $S_{k,\iota}$ denote the sum of the received signal power of the associated BSs on the k^{th} plane with link state ι, the approximate expression of the coverage probability of the typical user is

$$\begin{aligned} P_{\text{cov}} \approx& 1-\sum_{n=0}^{\lfloor\alpha\rfloor-1}\frac{(\beta\tau)^{-n}}{n!}\frac{\partial^n}{\partial s^n}\Bigg[\mathcal{M}_{S_{0,\text{N}}}(s) \\ &\times\prod_{k=1}^{K}\prod_{\iota\in\{\text{L},\text{N}\}}\mathcal{M}_{S_{k,\iota}}(s)\Bigg]_{s=-\frac{1}{\beta\tau}} \end{aligned}$$

$$-(\alpha-\lfloor\alpha\rfloor)\frac{(\beta\tau)^{-\lceil\alpha\rceil+1}}{(\lceil\alpha\rceil-1)!}\frac{\partial^{\lceil\alpha\rceil-1}}{\partial s^{\lceil\alpha\rceil-1}}\Bigg[\mathcal{M}_{S_{0,\mathrm{N}}}(s)\times\prod_{k=1}^{K}\prod_{\iota\in\{\mathrm{L},\mathrm{N}\}}\mathcal{M}_{S_{k,\iota}}(s)\Bigg]_{s=-\frac{1}{\beta\tau}},\tag{24}$$

where $\mathcal{M}_{S_{k,\iota}}(s)$ is the MGF of the received signal power $S_{k,\iota}$, and $\lfloor\cdot\rfloor$ is the floor operator.

Following the definition of MGF, we can obtain $\mathcal{M}_{S_{k,\iota}}(s)$ as shown in Corollary 2:

Corollary 2 Under the considered system model in Section 2, the MGF of the received signal power $S_{k,\iota}$ is given by

$$\mathcal{M}_{S_{k,\iota}}(s)=\begin{cases}\exp\Bigg(-\pi\lambda_0 E_{g_{0,\mathrm{T}}}\Big[\max\left\{D_{0,\mathrm{T}}^2,W_{0,\mathrm{T}}^2(g_{0,\mathrm{T}})\right\}\\ \times(1-\exp\left(sP_{\mathrm{t},0}K_{\mathrm{r}}\eta_{\mathrm{T}}g_{0,\mathrm{T}}\right.\\ \times\min\left\{D_{0,\mathrm{T}},W_{0,\mathrm{T}}(g_{0,\mathrm{T}})\right\}^{-\alpha_{\mathrm{T}}}))\\ +(-sP_{\mathrm{t},0}K_{\mathrm{r}}\eta_{\mathrm{T}}g_{0,\mathrm{T}})^{\frac{2}{\alpha_{\mathrm{T}}}}\\ \times\Gamma\left(1-\frac{2}{\alpha_{\mathrm{T}}},-sP_{\mathrm{t},0}K_{\mathrm{r}}\eta_{\mathrm{T}}g_{0,\mathrm{T}}\right.\\ \left.\times\min\{D_{0,\mathrm{T}},W_{0,\mathrm{T}}(g_{0,\mathrm{T}})\}^{-\alpha_{\mathrm{T}}}\right)\Big]\Bigg),k=0,\iota=\mathrm{T},\\ \exp\Bigg(-E_{g_{k,\iota}}\Big[\int_0^{\min\left\{\sqrt{D_{k,\iota}^2-H_k^2},\sqrt{W_{k,\iota}^2(g_{k,\iota})-H_k^2}\right\}}2\pi\\ \times\lambda_{\mathrm{A},\iota}p_\iota(z,H_k)z\Big(1\\ -\exp\Big(sP_{\mathrm{t},k}K_{\mathrm{r}}\eta_\iota g_{k,\iota}(z^2+H_k^2)^{-\alpha_\iota}\Big)\Big)\mathrm{d}z\Big]\Bigg),\\ k=1,2,...,K,\ \iota=\mathrm{L},\mathrm{N}.\end{cases}\tag{25}$$

Proof From the formulation of $S_{k,\iota}$, the MGF of the received signal power $S_{k,\iota}$ is mathematically written as

$$\mathcal{M}_{S_{k,\iota}}(s)=E\left[\exp\left(s\sum_{y_{k,j,\iota}\in\mathcal{B}_{\mathrm{a},k,\iota}}P_{\mathrm{t},k}K_{\mathrm{r}}\eta_\iota g_{k,j,\iota}\|y_{k,j,\iota}\|^{-\alpha_\iota}\right)\right].\tag{26}$$

For the case of TBSs (i.e., $k=0$ and $\iota=\mathrm{T}$), $\Psi_{0,\mathrm{N}}$ is an HPPP. Hence, following the Campbell theorem, $\mathcal{M}_{S_{0,\mathrm{T}}}(s)$ can be expressed as

$$\begin{aligned}\mathcal{M}_{S_{0,\mathrm{T}}}(s)&=\exp\Bigg(-E_{g_{0,\mathrm{T}}}\Big[\int_0^{D_{0,\mathrm{T}}}\big(1\\ &\quad-\exp\left(sP_{\mathrm{t},0}K_{\mathrm{r}}\eta_{\mathrm{T}}g_{0,\mathrm{T}}z^{-\alpha_{\mathrm{T}}}\right)\big)\\ &\quad\times1\left(z\le W_{0,\mathrm{T}}(g_{0,\mathrm{T}})\right)2\pi\lambda_{\mathrm{T}}z\mathrm{d}z\Big]\Bigg)\\ &=\exp\Bigg(-E_{g_{0,\mathrm{T}}}\Big[\int_0^{\min\{D_{0,\mathrm{T}},W_{0,\mathrm{T}}(g_{0,\mathrm{T}})\}}2\pi\lambda_{\mathrm{T}}z\\ &\quad\times\left(1-\exp\left(sP_{\mathrm{t},0}K_{\mathrm{r}}\eta_{\mathrm{T}}g_{0,\mathrm{T}}z^{-\alpha_{\mathrm{T}}}\right)\right)\mathrm{d}z\Big]\Bigg).\end{aligned}\tag{27}$$

For the case of ABSs, $\Psi_{k,\iota}$ is an in-HPPP and its distribution is described in Section 3.1. Similarly, $\mathcal{M}_{S_{k,\iota}}(s)$ can be expressed as

$$\begin{aligned}&\mathcal{M}_{S_{k,\iota}}(s)\\ &=\exp\Bigg(-E_{g_{k,\iota}}\Big[\int_0^{D_{k,\iota}}\left(1-\exp\left(\frac{sP_{\mathrm{t},k}K_{\mathrm{r}}\eta_\iota g_{k,\iota}}{\|y_{k,\iota}\|^{\alpha_\iota}}\right)\right)\\ &\quad\times1\left(\|y_{k,\iota}\|\le W_{k,\iota}(g_{k,\iota})\right)2\pi\lambda_{\mathrm{A},k}\\ &\quad\times p_\iota\Big(\sqrt{\|y_{k,\iota}\|^2-H_k^2},H_k\Big)\|y_{k,\iota}\|\mathrm{d}\|y_{k,\iota}\|\Big]\Bigg)\\ &=\exp\Bigg(-E_{g_{k,\iota}}\Big[\int_0^{\min\{D_{k,\iota},W_{k,\iota}(g_{k,\iota})\}}2\pi\lambda_{\mathrm{A},k}\\ &\quad\times\left(1-\exp\left(\frac{sP_{\mathrm{t},k}K_{\mathrm{r}}\eta_\iota g_{k,\iota}}{\|y_{k,\iota}\|^{\alpha_\iota}}\right)\right)\\ &\quad\times p_\iota\Big(\sqrt{\|y_{k,\iota}\|^2-H_k^2},H_k\Big)\|y_{k,\iota}\|\mathrm{d}\|y_{k,\iota}\|\Big]\Bigg).\end{aligned}\tag{28}$$

After sorting these formulas, we arrive at the results in Eq. (25).

4 Numerical results and discussion

In this section, the derived theoretical expression of the coverage probability of the 3D multilayer UAV-terrestrial HetNet based on the CoMP transmission scheme is verified by Monte-Carlo simulation, and the influence of the key system parameters in the network on the coverage performance is analyzed. The simulation results are generated from the Monte-Carlo simulation in MATLAB. Unless stated otherwise, the system parameters are set as follows: the transmit power of TBS $P_{\mathrm{t},0}=40$ dBm, the transmit power of ABS $P_{\mathrm{t},k}=32$ dBm, $K_{\mathrm{r}}=1$, $\alpha_{\mathrm{L}}=2.5$, $\alpha_{\mathrm{T}}=\alpha_{\mathrm{N}}=4$, $\eta_{\mathrm{L}}=1$, $\eta_{\mathrm{T}}=\eta_{\mathrm{N}}=0.2$, $m_{\mathrm{L}}=3$, $m_{\mathrm{T}}=m_{\mathrm{N}}=1$, $A=9.6117$, and $B=0.1581$ (Hu et al., 2019; Zeng et al., 2019c; Zhou et al., 2019). As for the thresholds related to the formulation of

CoMP sets, they are set as

$$\Theta_{k,\iota}=\begin{cases}10^{-3+\frac{-69.6}{10}}, & k=0,\\ 10^{-3+\frac{-30.1}{10}}, & k=1,2,...,K,\ \iota=\mathrm{L},\\ 10^{-3+\frac{-63.1}{10}}, & k=1,2,...,K,\ \iota=\mathrm{N}.\end{cases}$$

$$\tilde{\Theta}_{k,\iota}=\begin{cases}10^{-3+\frac{-69.6}{10}}, & k=0,\\ 10^{-3+\frac{-30.1}{10}}, & k=1,2,...,K,\ \iota=\mathrm{L},\\ 10^{-3+\frac{-63.1}{10}}, & k=1,2,...,K,\ \iota=\mathrm{N}.\end{cases}$$

4.1 Analysis validation

Fig. 2 shows the PDF of the simulation results and the analytical results of the aggregate interference. It can be seen that the simulation results of I_{agg} are generally consistent with the analytical results. Therefore, approximating I_{agg} as a Gamma random variable is feasible in the 3D HetNet considered in this work. In addition, it can be seen from the figure that when a new layer of the ABS network is added, the expectation and variance of the interference received by the typical user tend to increase.

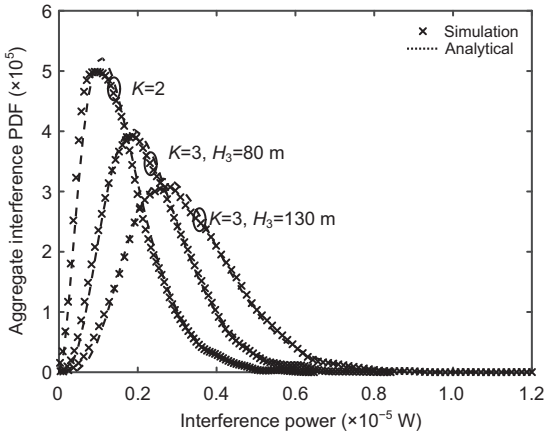

Fig. 2 Probability density function (PDF) of the interference I_{agg}

Fig. 3 shows the coverage probability v.s the SIR threshold τ for different network configurations. The figure shows that the simulation results and the analytical results fit closely, which validates the accuracy of the analytical results. By comparing the results when $K=3$ and $K=2$, we can see that when the SIR threshold is low, the coverage probability when $K=3$ is larger than that when $K=2$; while when the SIR threshold is high, the relationship is opposite. After adding a new layer of the ABS network, the number of activated cooperative BSs increases, but at the same time, the number of BSs that cause interference also increases. When the SIR threshold is low, more activated cooperative BSs are beneficial to increase the coverage probability of the typical user; when the SIR threshold is high, the coverage probability of the typical user is more affected by the interference from inactive BSs and non-cooperative BSs. In addition, it can be seen from Fig. 3 that under the same conditions and when threshold $\tau>-5$ dB, using CoMP can increase the coverage probability compared to that in the case not using CoMP. This shows that through the coordinated transmission of multiple BSs, co-channel interference is effectively reduced, which is beneficial to the improvement of coverage performance in the case of dense deployment of BSs.

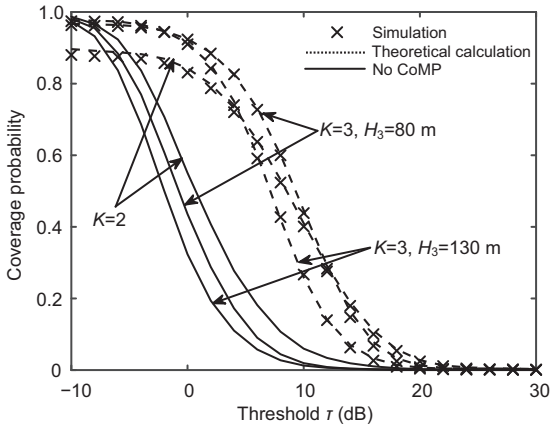

Fig. 3 Coverage probability v.s SIR threshold τ when $K=2$ and $K=3$ ($H_1=50$ m, $H_2=100$ m)

4.2 Effect of ABS height

For the convenience of discussion, we consider the situation with $K=2$. The ABSs deployed at the lower and higher altitudes are named as lower-altitude ABSs with height H_1 and higher-altitude ABSs with height H_2, respectively. Fig. 4 shows the coverage probability v.s the lower-altitude ABS height H_1 under different lower-altitude ABS densities when $H_2=110$ m and $\lambda_{\mathrm{A},2}=10^{-5}$ m^{-2} are considered. It can be seen that the coverage probability increases first and then decreases slowly as the height of the lower-altitude ABS increases. This trend can be explained as follows: when the ABS height increases from a lower value, the probability that the link from the activated cooperative BSs to the user is

in the LoS transmission condition increases, and the coverage performance improves. As the ABS height continues to increase, the activated cooperative BSs will be farther away from the user and the desired signal power received by the user will be smaller, so the coverage probability decreases.

Fig. 5 shows the relationship between the coverage probability and the height of the higher-altitude ABS H_2 under different densities of the higher-altitude ABS when $H_1 = 10$ m and $\lambda_{\mathrm{A},1} = 10^{-5}$ m^{-2} are considered. It can be seen that when H_1 is fixed, similar to Fig. 4, as H_2 increases, the coverage probability increases at first and then drops a little bit. This implies that there is also an optimal higher-altitude ABS flight height.

By comparing the variation range of the coverage probability with the ABS height in Figs. 4 and 5, it can be seen that the changes in the height of higher-altitude ABSs have a greater impact on the range of coverage probability than the changes in the height of lower-altitude ABSs. This indicates

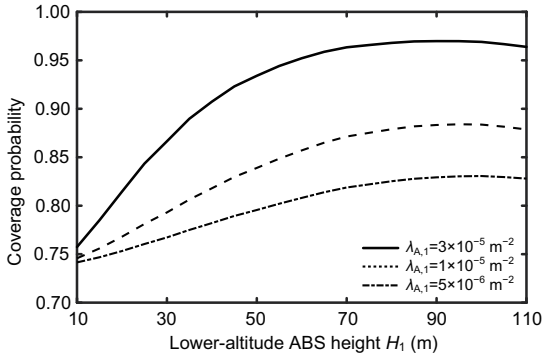

Fig. 4 Coverage probability under different lower-altitude ABS densities v.s lower-altitude ABS height H_1 ($H_2 = 110$ m, $\lambda_{\mathrm{A},2} = 10^{-5}$ m^{-2})

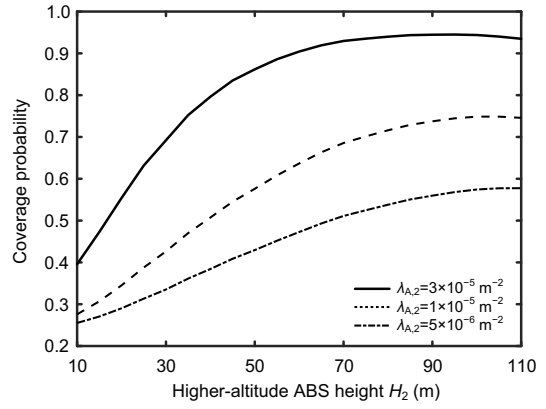

Fig. 5 Coverage probability under different higher-altitude ABS densities v.s higher-altitude ABS height H_2 ($H_1 = 10$ m, $\lambda_{\mathrm{A},1} = 10^{-5}$ m^{-2})

that the height of the higher-altitude ABSs is one of the main factors affecting the coverage probability of this HetNet.

4.3 Effect of BS density

Fig. 6 shows the coverage probability v.s the density of TBSs λ_{T} at different heights when $\lambda_{\mathrm{A},1} = \lambda_{\mathrm{A},2} = 10^{-5}$ m^{-2} and $H_2 = 50$ m are considered. It can be seen that the coverage probability increases as the density of TBSs increases. Fig. 7 shows the coverage probability at different heights v.s the density of ABSs $\lambda_{\mathrm{A},1}$ when $\lambda_{\mathrm{T}} = \lambda_{\mathrm{A},2} = 10^{-5}$ m^{-2} and $H_2 = 50$ m. Different from the TBS, it can be seen from Fig. 7 that the coverage probability first decreases and then increases with the increase of $\lambda_{\mathrm{A},1}$. This trend can be explained as follows: When the ABS density increases from a small value, due to the limited range of cooperative clusters and the height difference, the number of activated cooperative BSs increases slowly, while the increase in the interference caused by the increase of BS density (especially the interference from LoS-ABSs) has a larger impact on

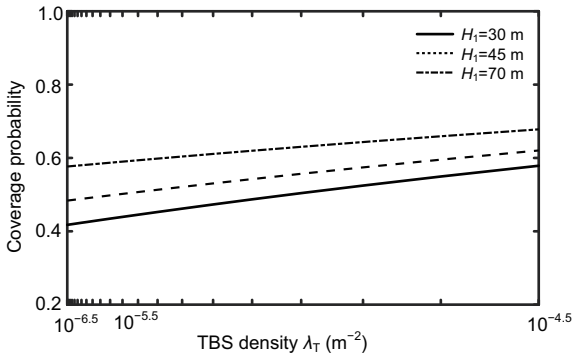

Fig. 6 Coverage probability v.s the density of the TBSs λ_{T} at different heights ($\lambda_{\mathrm{A},1} = \lambda_{\mathrm{A},2} = 10^{-5}$ m^{-2}, $H_2 = 50$ m)

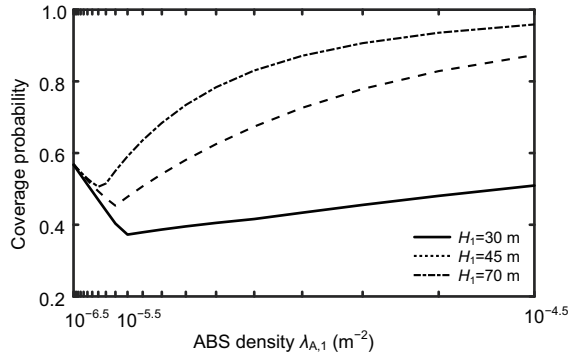

Fig. 7 Coverage probability at different heights v.s the density of ABSs $\lambda_{\mathrm{A},1}$ ($\lambda_{\mathrm{T}} = \lambda_{\mathrm{A},2} = 10^{-5}$ m^{-2}, $H_2 = 50$ m)

the coverage probability. As the density of ABSs continues to increase, the possibility of the activated cooperative BSs comprising LoS-ABSs increases, so the probability of providing the typical user with coverage under LoS transmission increases, and then the coverage probability increases. In addition, by comparing the variation range of each curve in Fig. 7, we can see that when the height of the ABSs increases, the variation range of the coverage probability with the density of the ABSs is larger, and the coverage probability with higher-altitude ABS is higher than that with lower-altitude ABS. This implies that the density of higher-altitude ABSs is a more important factor affecting the coverage probability of the multilayer UAV-terrestrial HetNet based on the CoMP transmission scheme.

By analyzing Figs. 6 and 7, we can find that when the BS density of the terrestrial or ABS network is larger, the coverage performance of the HetNet that adopts CoMP transmission is better. CoMP transmission can effectively reduce the interference from other BSs in a dense network environment, and a larger BS density is beneficial to the improvement of network coverage performance.

5 Conclusions

In this study, we have investigated the coverage performance of a 3D multilayer UAV-terrestrial HetNet with a CoMP scheme, in which multiple BSs with good channel conditions jointly transmit signals to users non-coherently. Using stochastic geometry, the mathematical framework to characterize the aggregate interference and evaluate the coverage performance of the considered HetNet has been developed. Based on this, the impact of key system parameters on the coverage performance has been studied. The results demonstrated the effectiveness of the CoMP scheme in the considered 3D HetNet under dense environments. It has also shown that the system parameters of the higher-altitude ABS influence mainly the coverage performance. Future work can be done to explore the design or the performance of more complicated cooperative architectures for the 3D UAV-terrestrial HetNet.

Contributors

Yifan JIANG designed the research and processed the data. Weihao WANG drafted the paper. Yifan JIANG helped organize the paper. Zesong FEI and Jing GUO revised and finalized the paper.

Compliance with ethics guidelines

Weihao WANG, Yifan JIANG, Zesong FEI, and Jing GUO declare that they have no conflict of interest.

References

3GPP, 2011. Coordinated Multi-point Operation for LTE Physical Layer Aspects, TR 36.819.

Akyildiz IF, Kak A, Nie S, 2020. 6G and beyond: the future of wireless communications systems. *IEEE Access*, 8:133995-134030. https://doi.org/10.1109/ACCESS.2020.3010896

Al-Hourani A, Kandeepan S, Lardner S, 2014. Optimal LAP altitude for maximum coverage. *IEEE Wirel Commun Lett*, 3(6):569-572. https://doi.org/10.1109/LWC.2014.2342736

Alzenad M, Yanikomeroglu H, 2019. Coverage and rate analysis for vertical heterogeneous networks (VHetNets). *IEEE Trans Wirel Commun*, 18(12):5643-5657. https://doi.org/10.1109/TWC.2019.2938168

Bor-Yaliniz I, Yanikomeroglu H, 2016. The new frontier in RAN heterogeneity: multi-tier drone-cells. *IEEE Commun Mag*, 54(11):48-55. https://doi.org/10.1109/MCOM.2016.1600178CM

Dang SP, Amin O, Shihada B, et al., 2020. What should 6G be? *Nat Electron*, 3(1):20-29. https://doi.org/10.1038/s41928-019-0355-6

Giordani M, Polese M, Mezzavilla M, et al., 2020. Toward 6G networks: use cases and technologies. *IEEE Commun Mag*, 58(3):55-61. https://doi.org/10.1109/MCOM.001.1900411

Guo J, Durrani S, Zhou XY, 2014. Characterization of aggregate interference in arbitrarily-shaped underlay cognitive networks. Proc IEEE Global Communications Conf, p.961-966. https://doi.org/10.1109/GLOCOM.2014.7036933

Haenggi M, 2012. Stochastic Geometry for Wireless Networks. Cambridge University Press, Cambridge, UK.

Haenggi M, Ganti RK, 2009. Interference in large wireless networks. *Found Trends Netw*, 3(2):127-248. https://doi.org/10.1561/1300000015

Hu HN, Gao Y, Zhang JL, et al., 2019. On the performance and fairness of LTE-U and WiFi networks sharing multiple unlicensed channels. Proc IEEE 30th Annual Int Symp on Personal, Indoor and Mobile Radio Communications, p.1-6. https://doi.org/10.1109/PIMRC.2019.8904396

Irmer R, Droste H, Marsch P, et al., 2011. Coordinated multipoint: concepts, performance, and field trial results. *IEEE Commun Mag*, 49(2):102-111. https://doi.org/10.1109/MCOM.2011.5706317

Jacovic M, Bshara O, Dandekar KR, 2018. Waveform design of UAV data links in urban environments for interference mitigation. IEEE 88th Vehicular Technology Conf, p.1-5. https://doi.org/doi: 10.1109/VTCFall.2018.8

Kishk M, Bader A, Alouini MS, 2020. Aerial base station deployment in 6G cellular networks using tethered drones:

the mobility and endurance tradeoff. *IEEE Veh Technol Mag*, 15(4):103-111. https://doi.org/10.1109/MVT.2020.3017885

Li B, Fei ZS, Dai YY, et al., 2018. Secrecy-optimized resource allocation for UAV-assisted relaying networks. Proc IEEE Global Communications Conf, p.1-6. https://doi.org/10.1109/GLOCOM.2018.8647437

Li B, Fei ZS, Zhang Y, 2019. UAV communications for 5G and beyond: recent advances and future trends. *IEEE Int Things J*, 6(2):2241-2263. https://doi.org/10.1109/JIOT.2018.2887086

Li Y, Miridakis NI, Tsiftsis TA, et al., 2020. Air-to-air communications beyond 5G: a novel 3D CoMP transmission scheme. *IEEE Trans Wirel Commun*, 19(11):7324-7338. https://doi.org/doi: 10.1109/TWC.2020.3010569

Liu L, Zhang S, Zhang R, 2019. CoMP in the sky: UAV placement and movement optimization for multi-user communications. *IEEE Trans Commun*, 67(8):5646-5658. https://doi.org/doi: 10.1109/TCOMM.2019.2907944

Mei WD, Zhang R, 2020. Cooperative downlink interference transmission and cancellation for cellular-connected UAV: a divide-and-conquer approach. *IEEE Trans Commun*, 68(2):1297-1311. https://doi.org/10.1109/TCOMM.2019.2955953

Qiu JF, Grace D, Ding GR, et al., 2019. Air-ground heterogeneous networks for 5G and beyond via integrating high and low altitude platforms. *IEEE Wirel Commun*, 26(6):140-148. https://doi.org/10.1109/MWC.0001.1800575

Saad W, Bennis M, Chen MZ, 2020. A vision of 6G wireless systems: applications, trends, technologies, and open research problems. *IEEE Netw*, 34(3):134-142. https://doi.org/10.1109/MNET.001.1900287

Sekander S, Tabassum H, Hossain E, 2018. Multi-tier drone architecture for 5G/B5G cellular networks: challenges, trends, and prospects. *IEEE Commun Mag*, 56(3):96-103. https://doi.org/10.1109/MCOM.2018.1700666

Singh S, Kumbhar A, Sichitiu ML, et al., 2018. Distributed approaches for inter-cell interference coordination in UAV-based LTE-advanced HetNets. IEEE 88th Vehicular Technology Conf, p.1-6. https://doi.org/doi: 10.1109/VTCFall.2018.8691002

Sun Y, Ding Z, Dai X, 2019. A user-centric cooperative scheme for UAV-assisted wireless networks in malfunction areas. *IEEE Trans Commun*, 67(12):8786-8800. https://doi.org/doi: 10.1109/TCOMM.2019.2944911

Tanbourgi R, Singh S, Andrews JG, et al., 2014a. Analysis of non-coherent joint-transmission cooperation in heterogeneous cellular networks. Proc IEEE Int Conf on Communications, p.5160-5165. https://doi.org/10.1109/ICC.2014.6884140

Tanbourgi R, Singh S, Andrews JG, et al., 2014b. A tractable model for noncoherent joint-transmission base station cooperation. *IEEE Trans Wirel Commun*, 13(9):4959-4973. https://doi.org/10.1109/TWC.2014.2340860

Wang HM, Huang KW, Tsiftsis TA, 2018. Base station cooperation in millimeter wave cellular networks: performance enhancement of cell-edge users. *IEEE Trans Commun*, 66(11):5124-5139. https://doi.org/10.1109/TCOMM.2018.2848910

Wang XL, Zhang HJ, Tian Y, et al., 2019a. Performance analysis of aerial base station assisted cooperative communication systems. Proc IEEE 89th Vehicular Technology Conf, p.1-5. https://doi.org/10.1109/VTCSpring.2019.8746388

Wang XL, Zhang HJ, Kim KJ, et al., 2019b. Performance analysis of cooperative aerial base station-assisted networks with non-orthogonal multiple access. *IEEE Trans Wirel Commun*, 18(12):5983-5999. https://doi.org/10.1109/TWC.2019.2941199

Wu HC, Tao XF, Zhang N, et al., 2018. Cooperative UAV cluster-assisted terrestrial cellular networks for ubiquitous coverage. *IEEE J Sel Areas Commun*, 36(9):2045-2058. https://doi.org/10.1109/JSAC.2018.2864418

Zeng Y, Wu QQ, Zhang R, 2019a. Accessing from the sky: a tutorial on UAV communications for 5G and beyond. *Proc IEEE*, 107(12):2327-2375. https://doi.org/10.1109/JPROC.2019.2952892

Zeng Y, Lyu J, Zhang R, 2019b. Cellular-connected UAV: potential, challenges, and promising technologies. *IEEE Wirel Commun*, 26(1):120-127. https://doi.org/10.1109/MWC.2018.1800023

Zeng Y, Xu J, Zhang R, 2019c. Energy minimization for wireless communication with rotary-wing UAV. *IEEE Trans Wirel Commun*, 18(4):2329-2345. https://doi.org/10.1109/TWC.2019.2902559

Zhang P, Peng MG, Cui SG, et al., 2022. Theory and techniques for "intellicise" wireless networks. *Front Inform Technol Electron Eng*, 23(1):1-4. https://doi.org/10.1631/FITEE.2210000

Zhang S, Liu J, 2018. Analysis and optimization of multiple unmanned aerial vehicle-assisted communications in post-disaster areas. *IEEE Trans Veh Technol*, 67(12):12049-12060. https://doi.org/10.1109/TVT.2018.2871614

Zhang ZQ, Xiao Y, Ma Z, et al., 2019. 6G wireless networks: vision, requirements, architecture, and key technologies. *IEEE Veh Technol Mag*, 14(3):28-41. https://doi.org/10.1109/MVT.2019.2921208

Zhou XH, Durrani S, Guo J, et al., 2019. Underlay drone cell for temporary events: impact of drone height and aerial channel environments. *IEEE Int Things J*, 6(2):1704-1718. https://doi.org/10.1109/JIOT.2018.2875166